Mechanical sensors

Helical-Shaped Graphene Tubular Spring Formed Within Microchannel for Wearable Strain Sensor With Wide Dynamic Range

Seval Oren[1], Halil Ceylan[2], and Liang Dong[1,3]

[1]Department of Electrical and Computer Engineering, Iowa State University, Ames, IA 50011 USA
[2]Department of Civil, Construction, and Environmental Engineering, Iowa State University, Ames, IA 50011 USA
[3]Microelectronics Research Center, Iowa State University, Ames, IA 50011 USA

Manuscript received August 27, 2017; revised September 24, 2017; accepted October 13, 2017. Date of publication October 17, 2017; date of current version November 1, 2017.

Abstract—This article reports on a helical spring-like piezoresistive graphene strain sensor formed within a microfluidic channel. The helical spring has a tubular hollow structure and is made of a thin graphene layer coated on the inner wall of the channel using an *in situ* microfluidic casting method. The helical shape allows the sensor to flexibly respond to both tensile and compressive strains in a wide dynamic detection range from 24% compressive strain to 20% tensile strain. Fabrication of the sensor involves embedding a helical thin metal wire with a plastic wrap into a precursor solution of an elastomeric polymer, forming a helical microfluidic channel by removing the wire from cured elastomer, followed by microfluidic casting of a graphene thin layer directly inside the helical channel. The wide dynamic range, in conjunction with mechanical flexibility and stretchability of the sensor, will enable practical wearable strain sensor applications where large strains are often involved.

Index Terms—Mechanical sensors, flexible mechanical sensors, microfluidics, helical spring, wearable electronics.

I. INTRODUCTION

Many functional nanomaterials and composites have recently been incorporated with elastomer substrates to realize flexible mechanical sensors [1]. These sensors often work by detecting subtle changes in electrical resistivity or permittivity of sensing materials in response to mechanical stimuli. For wearable sensor applications, such as body motion tracking [2], strain sensors often experience large tensile and compressive strains and thus require a wide dynamic range and high flexibility and stretchability [3]. Conventional strain sensors using rigid substrates, however, are unable to meet these requirements.

For substrate materials of wearable and flexible strain sensors, polydimethylsiloxane (PDMS) has been demonstrated as a promising elastomer substrate due to high stretchability and simple fabrication. Ecoflex is another substrate candidate material for strain sensors since it can be stretched by over 900% and return to its original state [4].

For sensing materials of wearable and flexible strain sensors, recent advances in nanomaterials have led to many candidate sensing materials in the form of nanoparticles, nanowires and nanotubes, as well as 2-D materials [5]–[15]. Among them, graphene possesses high piezoresistivity, electron mobility and flexibility [10]. As a result, many graphene-based flexible strain sensors have been developed by forming graphene patterns on the surface of elastomer substrate [14], [15] or using graphene based nanocomposites [16]–[18].

It should be pointed out that most of the existing graphene-based strain sensors use a planar structure. They are often realized on the surfaces of elastomer substrates. At large strains, the planar graphene elements tend to break, even though the elastomer substrates may still remain functional. In addition, most planar graphene sensors are not able to detect compressive strains. In order to enhance the dynamic range of strain sensors, wavy wrinkled micro/nanoscale structures have been created on the surfaces of elastomer substrates [16]–[18]. Carbon nanotube (CNT) array double helices have also been used as the main building block of a sensitive film to form a highly stretchable strain sensor on a thermoplastic elastomer substrate [19].

In this article, we demonstrate unique design and manufacturing of flexible strain sensors to obtain a wide dynamic range. The central core of the sensor is a helical-shaped tubular hollow structure made of graphene. The helically structured graphene is formed on the inner surface of a helical channel embedded inside a PDMS substrate. Due to the helical spring-like design, the sensor offers an improved dynamic range of strain along the axis of the spring and is able to respond to both compression and tension. In addition, unlike other graphene strain sensors manufactured using traditional techniques such as deposition, photolithography and etching, or new methods such as transfer printing, nanoimprint lithography and laser cutting [20]–[23], our graphene sensor uses a simple molding and refill process to realize *in situ* microfluidic casting of graphene layer directly inside the helical channel.

II. METHOD

Fabrication of the helical tubular graphene strain sensor takes four major steps, including i) embedding a helical coil into a precursor solution of elastomer [see Fig. 1(a)], ii) realizing a helical channel by removing the coil from cured elastomer [see Fig. 1(b) and (c)], iii) *in situ* microfluidic casting of graphene on the inner surface of the helical channel [see Fig. 1(d)], and iv) forming electrical contacts to external circuits. The detail of fabrication process is described below.

Initially, the precursor solution of PDMS was prepared by mixing Sylgard 184 silicone elastomer base and its curing agent (Dow Corn-

Corresponding author: L. Dong (e-mail: ldong@iastate.edu).
Associate Editor: Y. Suzuki.
Digital Object Identifier 10.1109/LSENS.2017.2764046

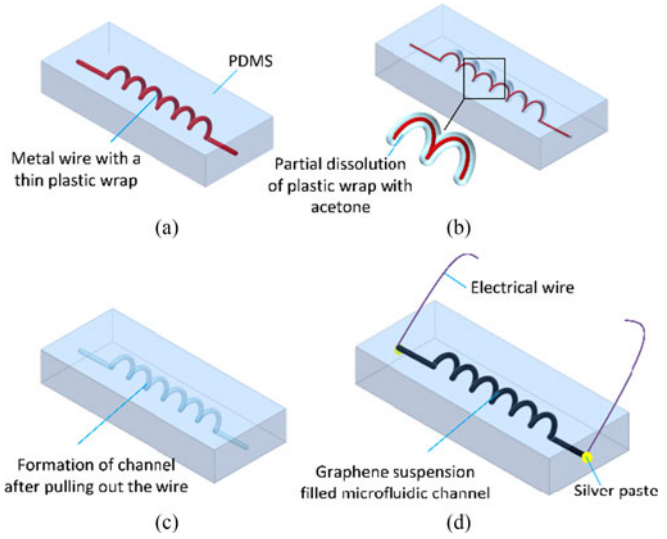

Fig. 1. Schematic representation of the fabrication process for the helical-shaped tubular graphene strain sensor.

ing, Auburn, MI) at a weight ratio of 10:1 and then were degassed in a vacuum desiccator for 20 min. Subsequently, a Tin-plated copper metal wire wrapped with a plastic coating (0.5 mm-diameter wrapping wire; Gauge 30) was manually winded around a 2.9 mm-diameter metal rod. The spacing between neighboring helix of the coiled wire was controlled by the alignment marks pre-labelled on the metal rod. The helical coil was taken off the rod, serving as a mold for the helical channel. Subsequently, the mold was fully immersed in the PDMS precursor solution. Here, the shape of the helical coil was determined by the following equations [24]:

$$L_o = \sqrt{(\pi D)^2 + S^2} \tag{1}$$

$$L_n = N L_o \tag{2}$$

$$L = N S \tag{3}$$

where D, S, L_o, N, L_n, and L correspond to the helix diameter ($D = 2.9$ mm), the distance between the neighboring turns ($S = 1.9$ mm), the circumference of each turn ($L_o = 9.3$ mm), the number of turns ($N = 6$), the total length of the coil in flat mode ($L_n = 55.8$ mm), and the straight end-to-end length of the coil ($L = 11.4$ mm). The helical coil was supported by two clips at its two ends before the PDMS precursor solution was poured over it. After thermally cured on a hotplate at 65 °C for 2 h, the cured PDMS embedded with the helical coil was placed in acetone for 2 h. As a result, the plastic wrap was partially dissolved by acetone, allowing easy pulling of the coil out of the PDMS. Therefore, a helical channel was obtained inside the elastomer. It should be noted that if a metal coil alone (without a plastic wrap) was used as the mold of the helical channel, it would be difficult to pull out the coiled metal due to a large friction between the metal and surrounding PDMS. On the other hand, a plastic wire alone (without a metal core) is not easy to be shaped into a coil. When serving as the mold, the plastic wire may be broken inside the PDMS during pulling.

Next, the *in situ* microfluidic casting approach was used to obtain a graphene layer on the inner wall of the helical channel. Here, aqueous solutions of graphene suspensions (20 mg/ml) were prepared by dispersing 20 mg graphene nanoplatelets (obtained by evaporation

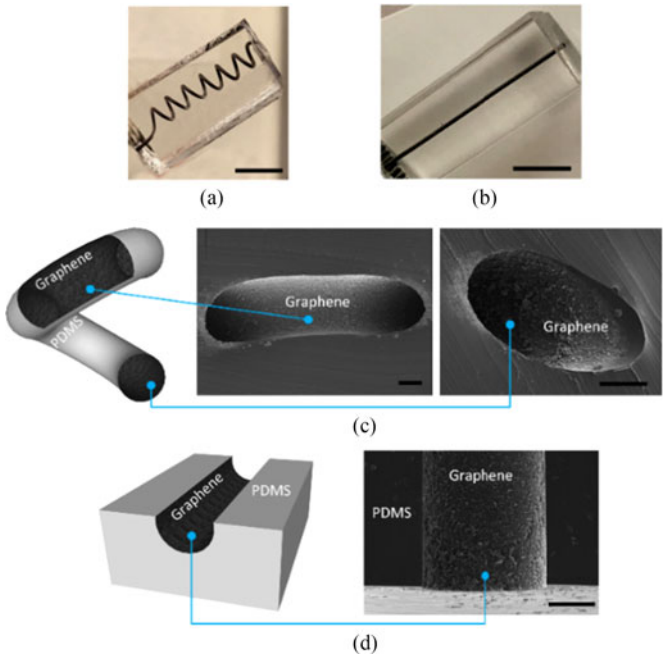

Fig. 2. (a) and (b) Fabricated tubular helical (a) and straight (b) graphene sensors. Scale bars represent 4 mm. (c) and (d) SEM images of the graphene coated inner surface of the helical (c) and straight (d) channels. Schematic for the helical and straight channels are shown to the left of (c) and (d), respectively. Scale bars represent 200 μm.

of acetate from the graphene dispersion purchased from Graphene Supermarket, Calverton, NY; SKU: UHC-NPD) in a 1 ml mixture of ethanol and deionized water at a volume ratio of 7:3, followed by sonication at room temperature for 400 min. The specific ethanol-to-water volume ratio was chosen because it could provide sufficient dispersion and maximum concentration of graphene nanoplatelets in the mixture [25]. After that, the helical channel was filled by injecting the prepared graphene suspension solution into the channel using a medical syringe (National Target; 10 ml volume). After drying at room temperature for 10 min and then at 90 °C for 5 min, a graphene layer (1.45 ± 0.24 μm) was casted on the inner surface of the channel. This *in situ* fabrication process was repeated twice to ensure a full graphene coverage on the inner wall. Next, electrical contacts of the graphene with two tin copper wires (Gauge 20) were realized with silver paste at the two ends of the channel. For comparison, a counterpart sensor with a straight channel was manufactured using the same fabrication process. The straight channel had the same diameter (0.5 mm) and end-to-end length (11.4 mm) as the helical channel.

III. RESULTS AND DISCUSSION

Fig. 2(a) and (b) show the fabricated helical and straight graphene sensors, respectively. Scanning electron microscopy (SEM) images in Fig. 2(c) and (d) demonstrate the formation of the graphene film on the inner walls of the channels. Because the graphene suspension solution contained 70% volume fraction of ethanol, the liquids could rapidly evaporate at 90 °C before the graphene nanoplatelets settled down in a direction, thus allowing casting a graphene layer on the inner wall in all radial directions.

To assess the mechanical properties of the sensors, the sensors were mounted on our home-made clamps. Different levels of tension and

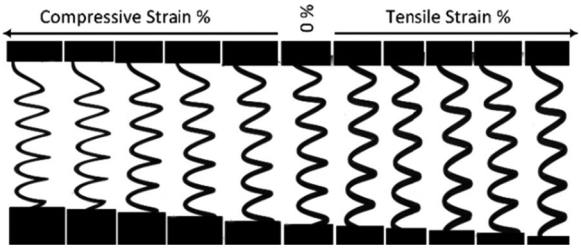

Fig. 3. Time-lapse images of the helical sensor under compression (left) and tension (right).

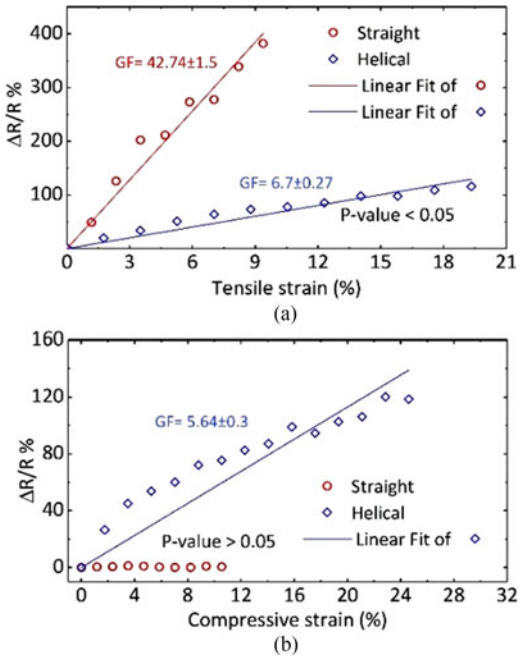

Fig. 4. Relative resistance changes of the helical and straight sensors under applied tensile (a) and compressive (b) strains.

compression were applied along the length direction of the sensors using a fully programmable motorized stage (LX-4000; Applied Scientific Instruments, Eugene, OR). The initial electrical resistances of the helical and straight sensors were 6 MΩ and 2.7 MΩ, respectively. An LCR meter (AT2817A; Applent Instruments, Jiangsu, China) was adopted to measure and record the resistance responses of the sensors to the applied strains. Fig. 3 presents the time-lapse images of the helical sensor when acting as a spring in response to different levels of compression and tension.

The testing of the sensor demonstrated some distinct features of the helical sensor when responding to tensile and compressive strains along the axis of the helical structure. Fig. 4(a) shows that the relative resistance changes (ΔR/R) of the helical and straight sensors increase almost linearly with applied tensile strains. The helical sensor could sustain to increasing tension up to 20% strain with a gauge factor of GF $= 6.7 \pm 0.27$ (obtained from the slope of the linear fitting curve). In contrast, the straight sensor provided a higher GF $= 42.8 \pm 1.5$ but could respond only up to 9% of tensile strain, beyond which the sensor would unrecoverable fail. The compression experiment also demonstrated that the helical design allowed extending the dynamic range of compressive strain measurements. Similarly, based on the slope of the fitting curve in Fig. 4(b), the GF of the helical sensor was

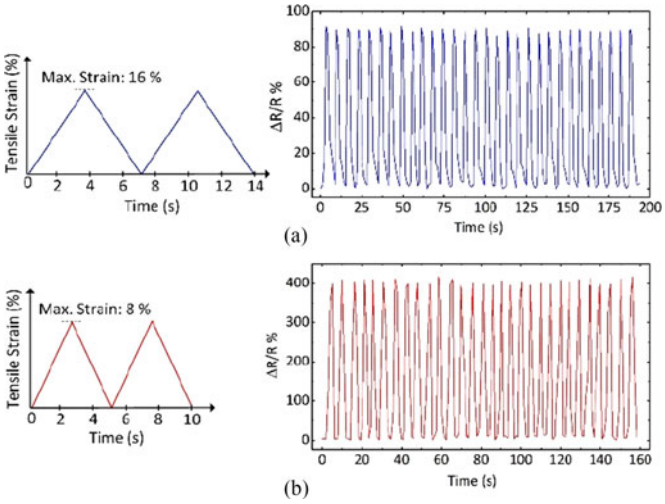

Fig. 5. Relative resistance changes of the helical (a) and straight (b) strain sensor responding to the repetition of 30 loading and unloading cycles. Sixteen percent and 8% tensile strains, each in a triangular waveform, were applied to the helical and straight sensors. The applied tensile strains are shown to the left of the corresponding response plots.

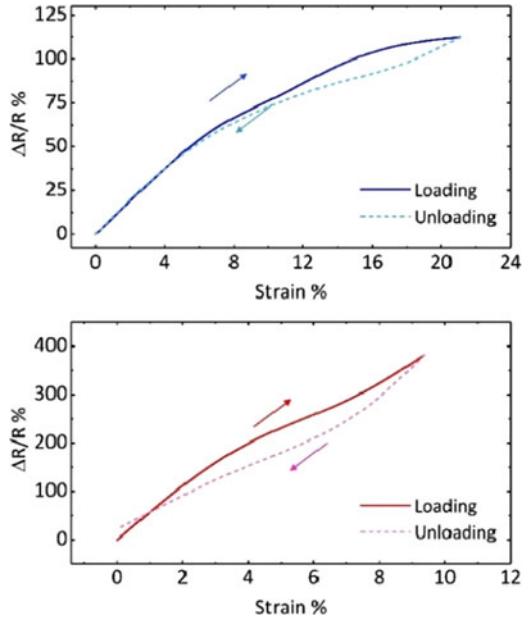

Fig. 6. Hysteresis of the helical (a) and straight (b) sensors.

found as 5.16 ± 0.3 under compression up to 24% strain, while the straight sensor showed little sensitivity to applied compressive strains.

Next, to verify stability and reversibility of the helical sensor, the sensor was repeatedly loaded and unloaded for 30 cycles (see Fig. 5). Here, 16% and 8% tensile strains, each in a triangular waveform, were applied to the helical and straight sensors, respectively, in the loaded state. Upon relaxation, the sensors returned to their initial resistance values, indicating good reversibility of the sensors. In addition, the helical and straight sensors exhibited a response time of ∼2.7 s and ∼1.1 s to the applied 16% and 8% tensile strains, respectively. The hysteretic behaviours of both the sensors were also investigated, during which the helical and straight sensors were stretched at the rate of 3.5% s^{-1} and then were released back to their initial positions at the same rate. Fig. 6 shows that the helical sensor exhibited a lower hysteresis than the straight sensor.

There is much room to improve the design of the sensor to achieve high sensitivity and wide dynamic range. For example, the critical parameters for the design of helical coil are determined by the following equations [26], [27]:

$$F = k\Delta l \tag{4}$$

$$k = \frac{Gd^4}{8ND^3} \tag{5}$$

where F, Δl, k, G, and d refer to the applied force, the force-induced change in the straight end-to-end length of the coil, the spring constant, the shear modulus of material, and the coil wire diameter, respectively. To increase the mechanical stretchability or dynamic range, one can increase both the diameter and number of helix while decreasing the coil wire diameter. This, however, will result in lowering the spring constant, and thus decreasing the sensitivity of the sensor. Therefore, while this work described here demonstrates proof-of-concept of the helical graphene strain sensor, one important future work is to explore the tradeoff between the sensitivity and stretchability of the device through systematic structural optimization. Although the previously reported strain sensor with the CNT array based double helices [19] exhibited higher stretchability than our sensor, it is nontrivial to realize the complex double helical nanostructures to build the sensor, and also it is unclear whether or not that sensor can respond to both tensile and compressive strains. In addition, other sensing nanomaterials, such as CNTs, may possibly be introduced into the channels to realize helical sensors, with tailored mechanic-electrical properties. Finally, by positioning aqueous graphene suspension solutions at different locations inside the channel [28] or selectively treating the surface chemical properties of the channel [29], it is possible to realize complex sensor structures inside the channel.

IV. CONCLUSION

We have demonstrated a novel helical-shaped tubular graphene strain sensor for the detection of large mechanical strains. This sensor is uniquely structured and manufactured in a way that allows a large dynamic range from 24% compressive strain to 20% tensile strain. The *in situ* microfluidic casting method is unique and simple, and allows easy coating of a graphene layer on the inner wall of the helical channel in all radial directions. The wide dynamic detection range, along with mechanical flexibility and stretchability, will benefit many wearable strain sensor applications such as real-time motion capture.

ACKNOWLEDGMENT

This work was supported in part by the Iowa Highway Research Board and the Iowa Department of Transportation and in part by the PSI Faculty Scholar Program at the Iowa State University.

S. Oren would like to thank the Turkish Council of High Education and Anadolu University for partial financial support. The authors would also like to thank K. Gopalakrishnan, P. Taylor, and S. Kim for discussions.

REFERENCES

[1] M. Amjadi, K. Kyung, I. Park, and M. Sitti, "Stretchable, skin-mountable, and wearable strain sensors and their potential applications: A review," *Adv. Funct. Mater.*, vol. 26, no. 11, pp. 1678–1698, 2016.

[2] Y. Jiao *et al.*, "Wearable graphene sensors with microfluidic liquid metal wiring for structural health monitoring and human body motion sensing," *IEEE Sensors J.*, vol. 16, no. 22, pp. 7870–7875, Nov. 2016.

[3] S. J. Park, J. Kim, M. Chu, and M. Khine, "Highly flexible wrinkled carbon nanotube thin film strain sensor to monitor human movement," *Adv. Mater. Technol.*, vol. 1, no. 5, 2016, Art. no. 1600053.

[4] S. Yang, P. Liu, M. Yang, Q. Wang, J. Song, and L. Dong, "From flexible and stretchable meta-atom to metamaterial: A wearable microwave meta-skin with tunable frequency selective and cloaking effects," *Sci. Rep.*, vol. 6, 2016, Art. no. 21921.

[5] J. Lee *et al.*, "A stretchable strain sensor based on a metal nanoparticle thin film for human motion detection," *Nanoscale*, vol. 6, no. 20, pp. 11932–11939, 2014.

[6] L. Yi *et al.*, "Nanoparticle monolayer-based flexible strain gauge with ultrafast dynamic response of acoustic vibration detection," *Nano Res.*, vol. 8, no. 9, pp. 2978–2987, 2015.

[7] S. Yao and Y. Zhu, "Wearable multifunctional sensors using printed stretchable conductors made of silver nanowires," *Nanoscale*, vol. 6, no. 4, pp. 2345–2352, 2014.

[8] M. Amjadi, A. Pichitpajongkit, S. Lee, S. Ryu, and I. Park, "Highly stretchable and sensitive strain sensor based on silver nanowire-elastomer nanocomposite," *ACS Nano*, vol. 8, no. 5, pp. 5154–5163, 2014.

[9] M. Amjadi, Y. Yoon, and I. Park, "Ultra-stretchable and skin-mountable strain sensors using carbon nanotubes-Ecoflex nanocomposties," *Nanotechnol.*, vol. 26, no. 37, 2015, Art. no. 375501.

[10] Q. Wang, W. Hong, and L. Dong, "Graphene 'microdrums' on a freestanding perforated thin membrane for high sensitivity MEMS pressure sensors," *Nanoscale*, vol. 8, no. 14, pp. 7663–7671, 2016.

[11] X. Li *et al.*, "Stretchable and highly sensitive graphene-on-polymer strain sensors," *Sci. Rep.*, vol. 2, 2012, Art. no. 395.

[12] S. Chun, Y. Choi, and W. Park, "All-graphene strain sensors on soft substrate," *Carbon*, vol. 116, pp. 753–759, 2017.

[13] C. Boland *et al.*, "Sensitive, high-strain, high-rate bodily motion sensors based on graphene–rubber composites," *ACS Nano*, vol. 8, no. 9, pp. 8819–8830, 2014.

[14] S.-H. Bae, Y. Lee, B. K. Sharma, H.-J. Lee, J.-H. Kim, and J.-H. Ahn, "Graphene-based transparent strain sensor," *Carbon*, vol. 51, pp. 236–242, 2013.

[15] B. Wang, B.-K. Lee, M.-J. Kwak, and D.-W. Lee, "Graphene/polydimethylsiloxane nanocomposite strain sensor," *Rev. Sci. Instrum.*, vol. 84, no. 1–4, 2013, Art. no. 105005.

[16] D. Y. Khang, H. Jiang, Y. Huang, and J. A. Rogers, "A stretchable form of single-crystal silicon for high-performance electronics on rubber substrates," *Science*, vol. 311, no. 5758, pp. 208–212, 2006.

[17] Y. Qi, J. Kim, T. Nguyen, B. Lisko, P. K. Purohit, and M. C. McAlpine, "Enhanced piezoelectricity and stretchability in energy harvesting devices fabricated from buckled PZT ribbons," *Nano Lett.*, vol. 11, no. 99, pp. 1331–1336, 2011.

[18] Y. Wang *et al.*, "Super-elastic graphene ripples for flexible strain sensors," *ACS Nano*, vol. 5, no. 5, pp. 3645–3650, 2011.

[19] C. Li *et al.*, "Flexible CNT-array double helices strain sensor with high stretchability for motion capture," *Sci. Rep.*, vol. 5, 2015, Art. no. 15554.

[20] A. Ng, Y. Wang, W. Lee, C. Lim, K. Loh, and H. Low, "Patterning of graphene with tunable size and shape for microelectrode array devices," *Carbon*, vol. 67, pp. 390–397, 2014.

[21] K. Yong, A. Ashraf, P. Kang, and S. Nam, "Rapid stencil mask fabrication enabled one-step polymer-free graphene patterning and direct transfer for flexible graphene devices," *Sci. Rep.*, vol. 6, no. 1, 2016, Art. no. 24890.

[22] J. W. Jeong *et al.*, "High-resolution nanotransfer printing applicable to diverse surfaces via interface-targeted adhesion switching," *Nat. Commun.*, vol. 5, 2014, Art. no. 5387.

[23] M. Hofmann, Y.-P. Hsieh, A. L. Hsu, and J. Kong, "Scalable, flexible and high-resolution patterning of CVD graphene," *Nanoscale*, vol. 6, no. 1, pp. 289–292, 2014.

[24] C. A. Balanis, *Antenna Theory–Analysis and Design*, 3rd Ed. New York, NY, USA: Wiley, 2005.

[25] W.-W. Liu, B.-Y. Xia, X.-X. Wang, and J.-N. Wang, "Exfoliation and dispersion of graphene in ethanol-water mixtures," *Frontiers Mater. Sci.*, vol. 6, no. 2, pp. 176–182, 2012.

[26] T. M. Atanackovic and A. Guran, "Hooke's Law," in *Theory of Elasticity for Scientists and Engineers*. Basel, Switzerland: Birkhauser, 2000, pp. 85–111, Ch. 3.

[27] Acxesspring.com, https://www.acxesspring.com/find-spring-constant-k-units-calculator.html

[28] L. Dong and H. Jiang, "Selective formation and removal of liquid microlenses at pre-determined locations within microfluidics through pneumatic control," *J. Microelectromech. Syst.*, vol. 17, no. 2, pp. 381–392, 2008.

[29] H. Yang and L. Dong, "Selective nanofiber deposition using a microfluidic confinement approach," *Langmuir*, vol. 26, no. 3, pp. 1539–1543, 2009.